Electronic Supplementary Information (ESI) for

A Baby-Step in Assembling and Integrating Components of Artificial Photosynthesis Device with Forced Heterojunctions Towards Improved Efficiency

Kranti N. Salgaonkar[1,2], Himanshu Bajpai[1,2], Nitin B. Mhamane[1,2], Naresh Nalajala[1], Inderjeet Chauhan[1,] Kavita Thakkar,[2,3] Kavita Joshi,[2,3] and Chinnakonda S. Gopinath[1,2,*]

[1]Catalysis and Inorganic Chemistry Division, CSIR-National Chemical Laboratory, Dr. Homi Bhabha Road, Pune 411 008, India.

[2]Academy of Scientific and Innovative Research (AcSIR), Ghaziabad 201002, India.

[3]Physical and Materials Chemistry Division, CSIR-National Chemical Laboratory, Dr. Homi Bhabha Road, Pune 411 008, India.

*Corresponding author. E-mail: cs.gopinath@ncl.res.in

This file contains

MM-SI - Materials and Methods

(a) Pd nanoparticles synthesis:

The synthesis of the Pd nanocubes with dominant (100) facets is synthesized as follows. In 8 mL of water, 105 mg of PVP (poly vinyl pyrrolidone), 60 mg of ascorbic acid, and 300 mg of KCl were added in 25 mL 3-neck round bottom flask (RBF), and kept at 363 K under constant stirring. After five minutes, 3 ml of water containing 57 mg of K_2PdCl_4 was added to the above solution and kept at the same temperature (363 K) for 3 h under constant stirring. After 3 h, the brown-black colored nanoparticle solution obtained was cooled to 298 K and collected in centrifuge bottles. Pd-nanoparticles was cleaned by centrifuging the solution with excess amount of acetone followed by ethanol/hexane mixture (1:5 ratio) at 10,000 rpm for 10 min. Final precipitate was dispersed in ethanol for further cleaning.[1] The synthesized Pd nanoparticle is coated as co-catalyst on conducting side of FTO plate and adjacent to BVT photoanode. 1 mg of Pd nanoparticle was dispersed in 1 ml ethanol. This solution was sonicated, just before coating on the device, by drop-casting method. 25 µl Pd solution (containing 25±3 µg) was coated on FTO plate by drop casting at 333 K for 1 cm^2 device and then heated to 363 K to remove any solvent molecules.

(b) Photocatalytic CO_2 reduction and control experiments:

1 cm^2 area BVT thin film photocatalyst device was prepared with 1 mg of $BiVO_4/TiO_2$ and integrated with Pd-co-catalyst. A digital photograph of the device is shown in Fig. S1. This photochemical device was kept in 30 ml of deionized water in a 50 ml capacity quartz reactor and sealed using an air-tight septum; water act as hydrogen source through photocatalytic water splitting. The reaction mixture was thoroughly saturated with CO_2 using 99.9% CO_2 gas (0.07% of nitrogen, and minor amount of oxygen and argon as impurities) for about 40 min. To dissolve the maximum amount of CO_2 in water, the reaction flask was placed in an ice bath (maintained at 278±1 K) at the time of saturation. pH of the solution was measured to be 6.2 indicating the slightly acidic nature of the solution due to CO_2 dissolution. Total amount of CO_2 dissolved in the water was measured through simple acid-base titration with NaOH solution (1.68 mmol). The reaction flask was illuminated under one sun condition as a function of reaction time. Product analysis was carried out periodically in this batch process. On the contrary, in the continuous process, CO_2 was continuously bubbled in to the liquid water present in the reactor

under illumination, and the reaction product has been analyzed periodically. Direct sunlight irradiation experiments were carried out on the terrace of National Chemical Laboratory (NCL), Pune premises for the unhindered access to sunlight throughout the day. Except O_2 and CO_2, no other gas phase product was observed; while liquid products are analyzed by HPLC method. NMR experiments were also carried out to ensure the HPLC results.

Several reference experiments, such as CRR with TiO_2 or $BiVO_4$ film, reaction without light or CO_2, were carried out. No significant product formation (> 2 μmol/h.cm^2) was observed with any of the reference experiments, underscoring the intrinsic CRR activity originates from visible-light absorption by $BiVO_4$ QDs assembled in the pores of TiO_2. With $BiVO_4/TiO_2$ film alone, some water oxidation occurs and it decreases with time. This observation hints the reaction is not sustainable since the electrons are not utilized for reduction and no hydrogen was observed. Although $BiVO_4$ film can be made by SILAR method directly on FTO plate, particle size was observed to be in the range of 1-1.5 μm, and hence the advantage of preparing QDs in TiO_2 mesopores could not be achieved. However, 35 μmol/cm^2 MeOH in 5 h was observed with Pd as co-catalyst; further, no formation of HCHO and other products was observed. With Pd/TiO_2 film, no CRR occurs in the presence of CO_2 in water; instead a small amount of H_2 (3.4 μmol/h.cm^2) was observed hinting water splitting reaction due to UV light absorption from sunlight.[2] Control experiments carried out reiterate that $BiVO_4$ QDs are critical for light absorption and heterojunction with TiO_2 is necessary for electron-hole separation.

(c) Material Characterization Methods

Fabricated BVT-AL photochemical device was characterized by various analytical methods. Newport Instruments 300 W xenon arc lamp fitted with an AM 1.5 filter was used to generate one sun condition in the laboratory. The wavelength dependent IPCE measurements were performed with Newport solar simulator (UUX 1404565) in CO_2 saturated water at 298 K. PEC experiments were carried out with 300 W xenon arc lamp fitted with an 1.5 AM filter connected with Gamry potentiostat. Electrochemical experiments were carried out with Gamry 3000 potentiostat. Diffuse reflectance UV–Vis measurement was carried with a Shimadzu spectrophotometer (model-UV2550). Powder X-ray diffraction (XRD) data was collected with a Pan Analytic X'pert pro dual goniometer diffractometer using Cu–Kα (1.5418 Å) radiation with a Ni filter. Field emission scanning electron microscopy (FESEM) and energy dispersive spectral

analysis (EDS) were performed on a FESEM system (FEI NOVA NANOSEM 450) equipped with EDS. HRTEM and chemical mapping of the material was conducted on a JEOL JEM F-200 HRTEM operating at 200 kV. Surface area and pore size/volume measurements were carried out with Quantachrome Quadrasorb unit. Gas chromatography analysis was performed with Agilent GC (7890) with Carbosieve S-II column and TCD detector. High performance liquid chromatography (HPLC, Agilent technologies, modal 1260 infinity) equipped with RI detector (at 40 °C) and H^+ Aminex column (305 mm × 7.8 mm) fitted with a guard column in series.

Photoelectrochemical and electrochemical Measurement: Electrochemical impedance spectroscopy (EIS) Nyquist plots and Transient photocurrent measurements under dark and light has been carried out under one sun illumination with 0.5 M Na_2SO_4 solution for photoanode with three electrode system; Ag/AgCl as reference electrode and Pt as counter electrode was used. Fabricated photoanode on FTO of 1 cm^2 was used as working electrode. The results obtained (with reference to Ag/AgCl) were converted to RHE using Nernst equation. Electrochemical CRR Linear sweep voltammogram measurement for co-catalyst Pd_{NC} has been carried out in 0.5 M $NaHCO_3$ saturated with N_2 or CO_2. 25 µg Pd_{NC} loaded on glassy carbon electrode was used as working electrode for photocatalytic CRR, with Ag/AgCl as reference and Pt as counter electrode. We also want to underscore that the best practices and careful measurements are adopted for the present work, as detailed in ref. 3.

(d) Quantification by NMR Method

This section elaborates the quantification of the product(s) by NMR using potassium hydrogen phthalate (KHP) as the internal standard. 450 µL of the reaction mixture was added to 130 µL deuterium oxide and 20 µL KHP used as the internal standard (corresponding to 1 mM solution in an NMR tube, where total volume is 600 µl). The concentration of liquid products formed in the above catalytic experiments was calculated by using the following formula: $n_x/n_y = I_x/I_y \times N_y/N_x$.

$$\frac{n_x}{n_y} = \frac{I_x}{I_y} \times \frac{N_y}{N_x}$$

Here, n_x represents the molar concentration of KHP, I_x represents the integral area in ^{1}H NMR spectrum for KHP, N_x is the number of nuclei of KHP, and n_y is calculated from the above formula for the liquid product, I_y for integral area of the product formed, and N_y is the number of nuclei of product peak.

Reaction condition: Products obtained from BVT CRR batch type reaction after 1 h reaction under one sun condition.

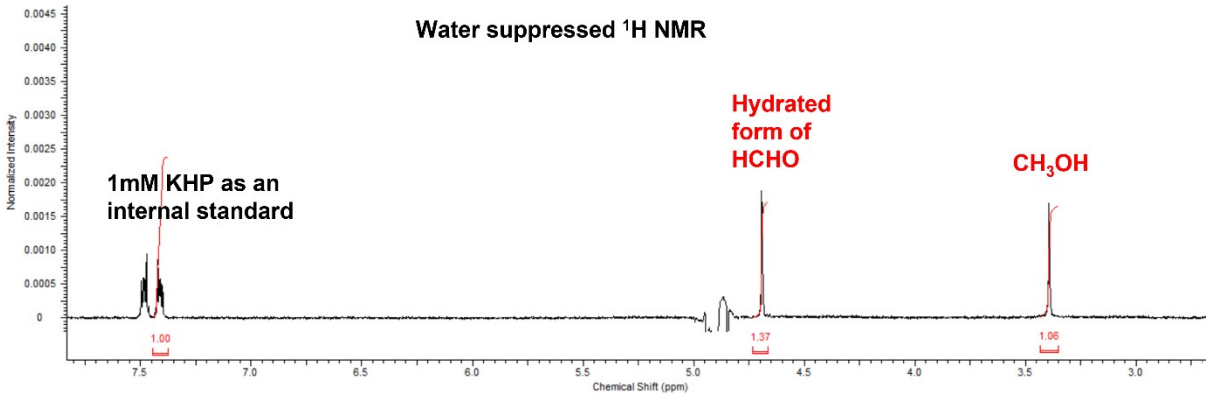

Figure S1: NMR spectra with the products obtained after the co-conversion of water and CO_2 in the presence of 1 cm^2 BVT-AL device. Water suppression sequence was employed.

Calculation of concentration of Methanol from NMR

$$= \frac{1.06}{1} \times \frac{2}{3} \times 1 = 0.69\ mM\ in\ 0.6\ ml\ of\ solution$$

It is to be noted that KHP peaks split into two equal doublets and integrated area under only one doublet is accounted for two protons; while methanol peak at 3.35 ppm corresponds to three protons, and hence the ratio becomes 2/3.

Hence concentration of methanol in 450 µl of sample solution becomes= 0.93 mM; thus total concentration of methanol in 30 ml reactor becomes 0.93 mM.

To convert mM to µmol: Mol. Wt of methanol is 32.04 g.

Reference: 32.04 mg of Methanol in 1000 ml solution = 1 mM methanol

Hence 30 ml of methanol solution = 0.97 mg Methanol= 1 mM methanol

Thus in 30 ml of CRR solution = 0.90 mg of Methanol = 0.93 mM methanol

As we know 1 mmol =32.04 mg of methanol

0.90 mg of methanol corresponds to $= \frac{0.90}{32.04} = 0.028\ mmol = 28\ \mu mol$

Similar calculation is followed for detection of formaldehyde and its found to be 3.64 mM (109 µmol). The values obtained from NMR are similar to values obtained by HPLC analysis of products, and indeed above reaction solution analyzed by HPLC provides 29 µmol and

formaldehyde to be 108 µmol, which is within ±5% error limit. This is the quantification method adopted throughout the analysis of the current manuscript.

e) Solar to fuel efficiency (STF) and Apparent quantum efficiency (AQE) calculations:

Calculation details are given for direct sunlight experiments under batch and continuous modes. It is to be noted that the calculations given below are carried out with the results obtained from 1 cm^2 area device, which contains ~25 µg of $BiVO_4$, and the product yield is given in µmol/h. Energy output to energy input ratio gives the STF[3].

For batch mode experiments:

$$\text{STF} = \frac{CH_3OHyield \times \Delta G}{P_{total} \times Area}$$

Average power density (P_{total}) measured is assumed to be 65 mW/cm^2 and irradiation area is 1 cm^2. The average rate of MeOH formation observed experimentally in direct sunlight and batch mode is 56 µmol/h (Table 1 – Main manuscript). ΔG for methanol formation from CO_2 is 638.73 kJ/mol.

$$\text{STF} = \frac{56 \times 638.73}{65 \times 3600 \times 1} \times 100 = 15.3\%$$

$$\text{STF} = \frac{HCHOyield \times \Delta G}{P_{total} \times Area}$$

Rate of formation of HCHO is 72 µmol/h (Table 1 – Main manuscript); ΔG of HCHO formation from CO_2 is 512 kJ/mol;

$$\text{STF} = \frac{72 \times 512}{65 \times 3600 \times 1} \times 100 = 15.8\%$$

For Continuous mode:

Solar to fuel efficiency

Rate of formation of methanol and HCHO are 71 µmol/h and 86 µmol/h, respectively (Table 1 – main manuscript).

$$\text{STF (MeOH)} = \frac{71 \times 638.73}{65 \times 3600 \times 1} \times 100 = 19.4\%$$

STF (HCHO) = $\frac{86 \times 512}{65 \times 3600 \times 1} \times 100 = 18.8\%$

Since both products are forming simultaneously, the total STF (either in terms of total CO_2 conversion or both products together) is 31.1 % (batch mode) and 38.2 % in continuous mode at a P_{total} = 65 mw/cm^2.

AQE :

The wavelength dependent AQE was calculated using monochromatic light source. Newport light source (300W Xe lamp) was used along with Newport 74125 monochromator to obtain the monochromatic wavelengths; Newport-1918-R power meter was used to measure the incident light intensity.

AQE was estimated from equation= $\frac{Number\ of\ \ reacted\ electron}{Number\ of\ incident\ photon} \times 100$

Thus AQE for present reaction is =

$$\frac{[(6\ \times\ No.\ of\ \ CH3OH\ molecules) + (4\ \times\ No.\ of\ HCHO\ molecules) \times Avagadro}{Number\ of\ incident\ photons\ x\ t} \times 100$$

Number of incident photon= $\frac{P\lambda}{hc}$

Where, P = power density of the incident monochromatic light (W/cm^2), t (s) =duration of the incident light illumination, λ(m) = wavelength of the incident monochromatic light; h is Planck's constant, and c is the speed of light (m/s) .

Number of incident photon at 410 nm = $\frac{0.040 \times 410 \times 10^{-9}}{6.626 \times 10^{-34} \times 3 \times 10^{8}} = 0.83 \times 10^{17}$ photon per sec.

Yield of methanol and formaldehyde at 410 nm found to be 5.19 and 8.39 μmol/h, respectively.

AQE= $\frac{(6 \times 5.19) + (4 \times 8.39)\ \times 10^{-6} \times\ 6.022\ \times\ 10^{23}}{0.83\ \times 10^{17} \times 3600} \times 100$ = 13%

Similarly, AQE was calculated for 440 and 490 nm too.

f) A semi-quantitative look at the number of $BiVO_4$-TiO_2 heterojunctions:

As per TEM images and pore size distribution measured, mesopores of 2.3, 3, 4 and 5.7 nm diameter are found, apart from micropores. To make the number of heterojunctions calculations simplified, following valid assumptions are made. It is assumed that titania have only 2.5 and 4 nm diameter pores. 2.5 and 4 nm diameter pores are filled with $BiVO_4$ in the weight ratio of 1:4 (5 µg : 20 µg), and how many mesopores can be filled with 25 µg of $BiVO_4$ in TiO_2. Apart from filling with the full $BiVO_4$ unit cells, part unit cells were also considered on the periphery of $BiVO_4$ particle to make the fully packed pores, since crystalline solid should have an extended lattice. In view of these assumptions, we suggest a generous error limit up to 20 % for the values given in this section.

Volume of one 4 nm sphere is calculated to be 33.51 nm^3. Experimental value for monoclinic $BiVO_4$ is a=5.194 Å, b=5.09 Å, c=11.697 Å, and hence the volume is 0.3092 nm^3.[4-5] It is calculated that 4 nm mesopore accommodates 108 unit cells of $BiVO_4$. One $BiVO_4$ unit cell contains 4 molecules of $BiVO_4$, and hence in 4 nm mesopore can accommodate 432 molecules of $BiVO_4$. Similarly, it is calculated for 2.5 nm pore too. 8.18 nm^3 volume of one 2.5 nm pore can accommodate 26.47 unit cells or 106 molecules of $BiVO_4$.

1 mole (or 6.02×10^{23} molecules) of $BiVO_4$ = 324 g.,

and hence, 432 molecules of $BiVO_4$ has 23.25×10^{-20} g weight in one 4 nm pore of $BiVO_4$

It is assumed that one TiO_2 mesopore with $BiVO_4$ QD in it generates one heterojunction; however, it could be more, which is not considered for the present calculation. Further, $BiVO_4$ filled micropores of titania is also not considered for this calculations.

$$\text{Number of heterojunctions (by 4 nm)} = \frac{20 \times 10^{-6}}{23.25 \times 10^{-20}} = 86 \times 10^{12}$$

$$\text{Number of heterojunctions (by 2.5 nm)} = \frac{5 \times 10^{-6}}{5.702 \times 10^{-20}} = 88 \times 10^{12}$$

86 trillions of 4 nm diameter $BiVO_4$ particles with a weight of 20 µg was accommodated in titania pores generates a minimum of 86 trillion heterojunctions; similarly, another 88 trillion $BiVO_4$ particle of 2.5 nm in diameter weighing 5 µg generates a minimum of 88 trillion heterojunctions. Hence a total of 174 trillion heterojunctions could be possible in 1 cm^2 device with 1 mg BVT photoanode material.

From the pore volume analysis of P25-TiO_2 it is known that the pore volume 0.18 ml/g and this translates to 0.18×10^{-3} cm^3/mg. By assuming 80 % (20 %) pores are spherical in shape and 4 nm (2.5 nm) in diameter, each pore volume is estimated to be 33.51 nm^3 (8.18 nm^3). A simple back calculation reveals that 1 mg of TiO_2 is expected to have 5.4×10^{15} mesopores of 4 and 2.5 nm diamter in 4:1 ratio occupies a volume of 0.18×10^{-3} cm^3 .

From 5.4×10^{15} pores (5.4 quadrillion) of TiO_2, only 0.174×10^{15} pores (0.174 quadrillion) are occupied by $BiVO_4$ QDs. This in turn indicates that 3.2 % of pores are occupied by $BiVO_4$ QDs present in the pores of 1 mg of TiO_2. Indeed, present semi-quantitative calculation underscores that there is plenty of scope to improve the activity of this catalyst by fine tuning the synthetic strategy further.

---

g) ToF calculations and Number of Photon Absorption per sec.cm²

Turn Over Frequency (ToF) = $\frac{molesofproductsformed}{moleofcatalyst}$

25 µg of $BiVO_4$ corresponds to 0.077×10^{-6} moles of $BiVO_4$. Total product (methanol + formaldehyde) formed is 157 µmol/h in direct sunlight continuous mode:

Hence ToF = $\frac{157 \times 10^{-6} \times 6.023 \times 10^{23}}{0.077 \times 10^{-6} \times 6.023 \times 10^{23} \times 3600} = 5.67 s^{-1}$

ToF for Photon to Chemical (P2C) conversion (ToF_{P2C}) was also calculated, as shown below.

For continuous mode reaction 71 µmol/h methanol is produced with 25 µg of $BiVO_4$. In this process, a total of 6 electrons are consumed for the formation of one methanol molecule. In other words, 71×6= 426 µmol/h electrons are needed.

$CO_2 + 6H^+ + 6e^- \rightarrow CH_3OH + H_2O$

Hence effective photons consumed/sec = $\frac{426 \times 10^{-6} \times 6.023 \times 10^{23}}{3600} = 6.9 \times 10^{16} \frac{photons}{s.cm^2}$

Similarly 86 µmol/h formaldehyde is produced with 25 µg of $BiVO_4$. A total of 4 electrons are consumed per formaldehyde molecule. i.e. 86×4= 344 µmol/h electrons are needed.

$CO_2 + 4H^+ + 4e^- \rightarrow HCHO + H_2O$

Hence effective photon consumed/sec = $\frac{344 \times 10^{-6} \times 6.023 \times 10^{23}}{3600} = 5.76 \times 10^{16} \frac{photons}{s.cm^2}$

Total effective Photon absorption/sec = $(6.9 + 5.76) \times 10^{16} = 12.66 \times 10^{16} \frac{photons}{s.cm^2}$

$ToF_{P2C} = \frac{Totalnumberofphotonseffectivelyabsorbedproduceproducts}{moleofcatalyst}$

Hence $ToF_{P2C} = \frac{12.66 \times 10^{16}}{0.077 \times 10^{-6} \times 6.023 \times 10^{23}} = 2.73 s^{-1}$

$\frac{Totalphotonsabsorbed}{no.ofBiVO4filledpores} = \frac{12.66 \times 10^{16}}{174 \times 10^{12}} = 727.6$

727.6 photons absorbed per particle of $BiVO_4$, assuming 4 and 2.5 nm $BiVO_4$ particle size has no effect on light absorption and they behave identical.

Nonetheless, to arrive at the semi-quantitative number of photons absorbed per 4 nm $BiVO_4$ particle as well as per $BiVO_4$ molecule, the following assumption is made. All the $BiVO_4$ filled TiO_2 pores are uniformly 4 nm in size; this lead to the conclusion that to accommodate 25 μg of $BiVO_4$, 110 trillion 4 nm TiO_2 pores would be required.

$\frac{Totalphotonsabsorbed}{no.ofBiVO4filledpore} = \frac{12.66 \times 10^{16}}{110 \times 10^{12}} = 1150.9$

$\frac{1150.9}{108.4} = 10.62 = Numberofphotonsabsorbed \in onesecperunitcellofBiVO_4$

$\frac{1150.9}{433.6} = 2.65 = Numberofphotonsabsorbed \in onesecpermoleculesofBiVO_4$

Four $BiVO_4$ molecules is present in one monoclinic unit cell, and hence 4 nm of $BiVO_4$ spherical particle contains 433.6 molecules of $BiVO_4$. 4 nm sphere of $BiVO_4$ accomodates 108.4 unit cells of $BiVO_4$.

h) **<u>Computation Details</u>**

All the calculations are carried out within the Kohn-Sham formalism of density functional theory (DFT). Projector Augmented Wave potential is used, with Perdew-Burke-Ernzerhof (PBE) approximation for the exchange-correlation and generalized gradient approximation, as implemented in plane wave, pseudo-potential based code, Vienna Ab initio Simulation Package (VASP).[6-8] van der Waals interactions are applied to account for the dispersion effect as implemented in the Grimme approach (DFT-D2).[9] Bulk CIfs for anatase TiO_2, monoclinic $BiVO_4$, and Pd are obtained from the Materials Project.[10] The lattice constants are calculated and verified with the experimentally measured ones (details in Tab. S1). As observed in the

experiments, we consider TiO_2(101), $BiVO_4$(121) and Pd(100) facets for modeling the hetero-structure. For TiO_2, a slab of 3x1 with three layers is cleaved along the (101) direction using VNL,[11] with the bottom layer fixed to mimic bulk. For $BiVO_4$ and Pd, slabs of 1x1 (3 layers) and 4x4 (4 layers) are cleaved along (121) and (100) directions, respectively. A Monkhorst-Pack grid of 2x2x1 is used which resulted in 2 k-points in the IBZ. A vacuum of 20.0 Å is employed along the z-direction to avoid interaction between adjacent images. Geometry optimization is carried out with a force cutoff of 0.05 eV/Å on the unfixed ions, and the total energies are converged below 10^{-4} eV for each SCF cycle. PBE and Hyed−Scuseria−Ernzerhof (HSE06) exchange-correlation functionals[12,13] are adopted to calculate the band gap. The site-specific density of states and Mulliken charges are calculated with denser k-mesh using LOBSTER.[14] Formation energy (E_{form}) of the hetero-structure is determined using the equation: $E_{form} = E_{Hetero} - [E_{S1} + E_{S2}]$, E_{Hetero} is the energy of the resultant hetero-structure and E_{S1} and E_{S2} are the energies of the surfaces interfaced to form the hetero-structure. To quantify the interaction between surface and adsorbate, we calculate the adsorption energy (E_{ads}) using the formula: $E_{ads} = E_{system} - [E_{surface} + E_{adsorbate}]$ where E_{system} is the energy of the surface plus the adsorbate, $E_{surface}$ is the energy of the bare surface, $E_{adsorbate}$ and is the energy of the adsorbate.

Figure S2: 1 cm^2 $BiVO_4/TiO_2$ (BVT) photoanode with Pd nanoparticle as cathode (BVT-AL) wireless photocatalytic device. Just for the clarity of the Pd-particles in the photograph, deliberately large amount of Pd is coated; In the normal device, about ~10% is coated, compared to what is seen.

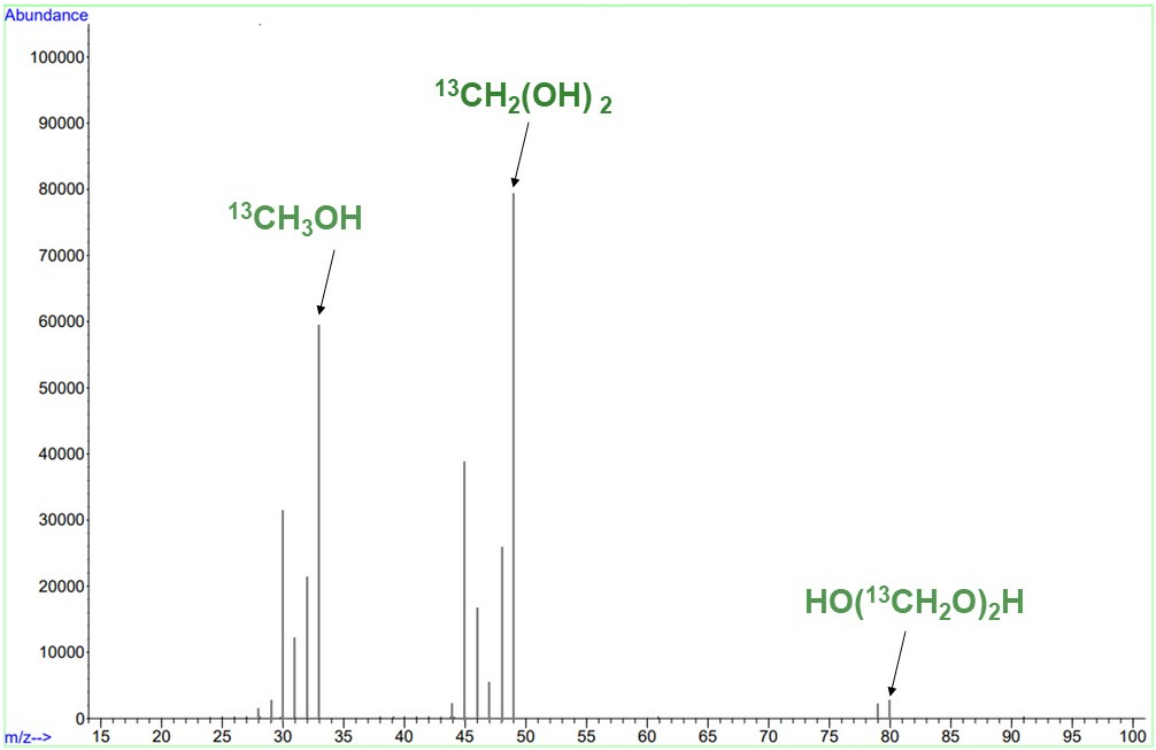

Figure S3. Mass spectrum recorded to identify the products obtained with $^{13}CO_2$ as the reactant, after 5 h of illumination under one sun condition with Pd-BVT catalyst. About 1% of dimeric form of formaldehyde (m/z = 80 and 79) is also observed, along with hydrate form of formaldehyde and methanol. There is no other (dissolved) products, such as, $^{13}CH_4$, were observed. No other gaseous products were observed in gas chromatographic analysis.

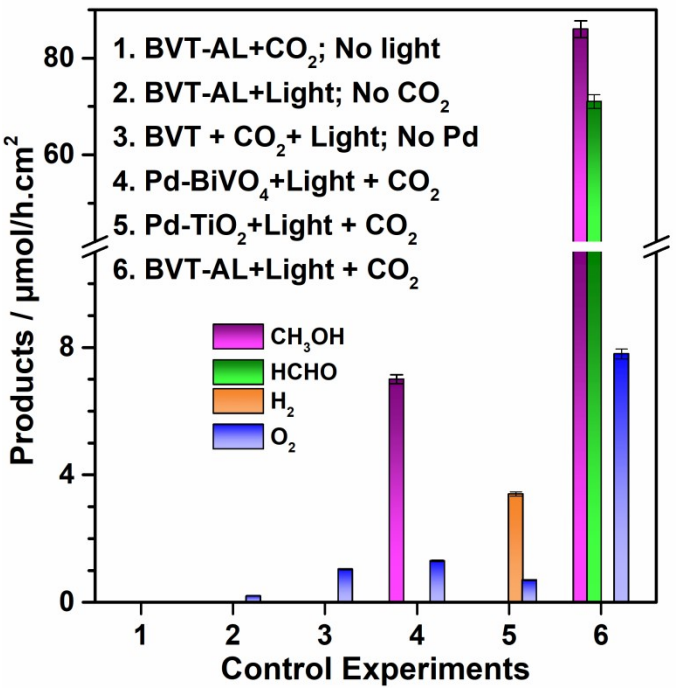

Figure S4: Graphical representation of several control experiments carried out for CRR study, as described in the main manuscript, but in the absence of one of the critical component. Unless all the components are present, as shown in 6, no meaningful reaction occurs. Apart from the experiments shown here, only CO_2 was introduced into the reactor without any catalyst, but in the presence of light and no product was observed. This reiterates that there is no error, such as impurity carbon components leading to any C1-oxygenate, in carrying out the reactions. $^{13}CO_2$ labeled experimental results shown in Fig. 2 in the main manuscript reiterates our observation are exclusively due to artificial photosynthesis, and not by any impurities.

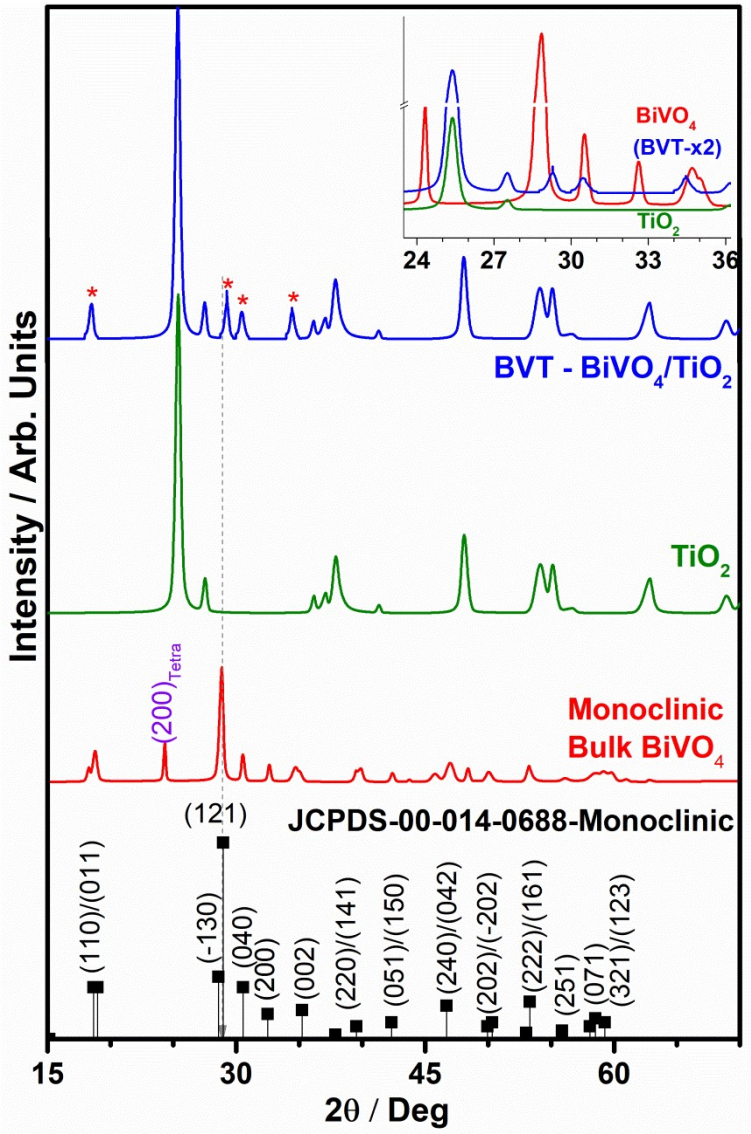

Figure S5: Powder X-ray diffraction (PXRD) pattern of bulk $BiVO_4$, commercial P25-TiO_2, and $BiVO_4/TiO_2$. JCPDS pattern for $BiVO_4$ is also given for reference. Only four facets of $BiVO_4$ is clearly identified in BVT film, and indicated by *. The anatase and rutile phase of TiO_2 were distinctly observed in both TiO_2 and BVT films, while many low intensity features of $BiVO_4$ is not observed in BVT. (200) facet of tetragonal $BiVO_4$ is identified at 24.5 deg.; however it is not present in BVT. Inset shows the enlarged version of PXRD patterns of all three materials, mainly to show the major shift (0.45 deg) with (121) facet in BVT, compared to bulk BV. (121) facet shows the maximum shift, while (200) and (002) facets show a minor expansion (with shift to lower angle by 0.18 deg) in BVT, compared to bulk $BiVO_4$; (040) and (011) facets are unaffected.

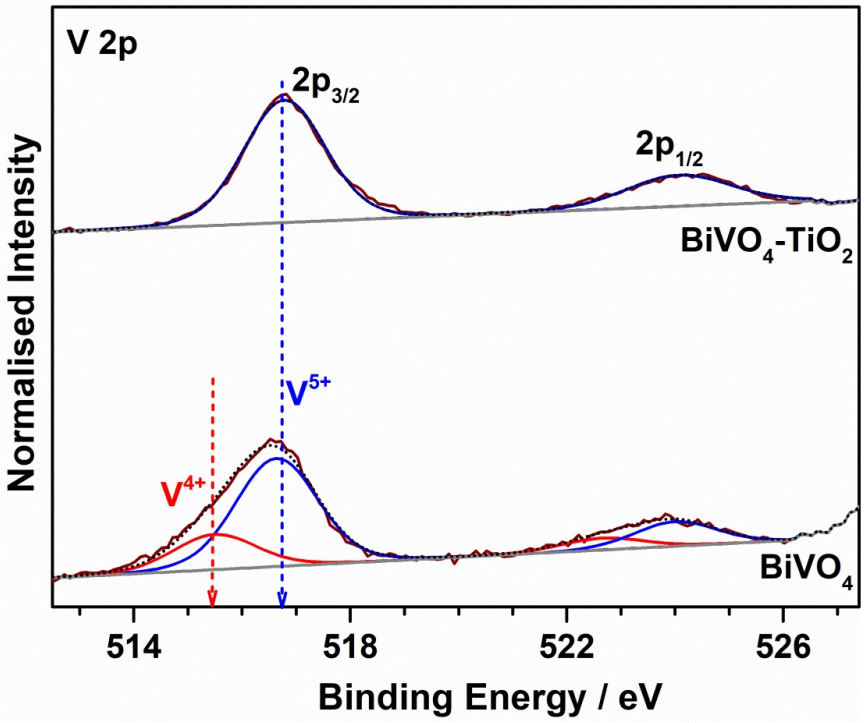

Figure S6: V 2p core level XPS recorded for bulk $BiVO_4$ and BVT; while the former shows mixed valent vanadium oxidation states (4+ and 5+), the latter shows only 5+ oxidation state.

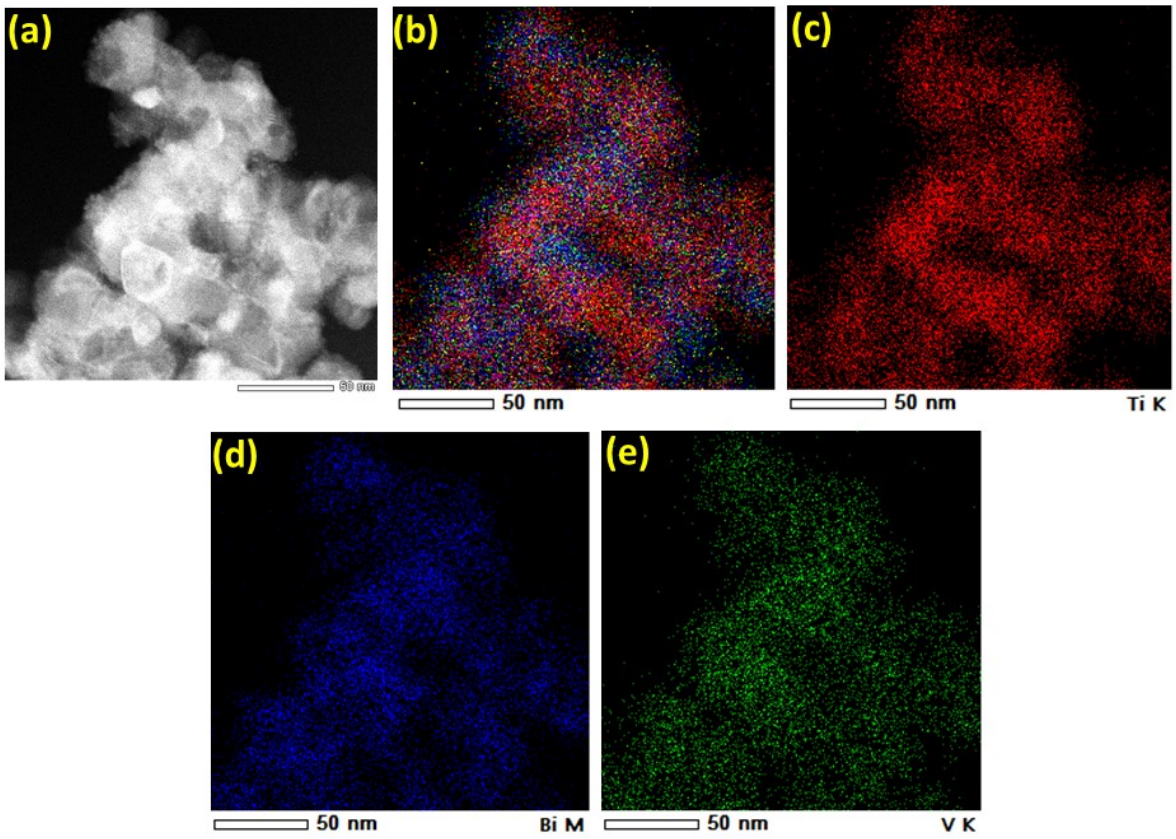

Figure S7: STEM for elemental mapping of $BiVO_4/TiO_2$ photoanode has been carried out. (b) Combination of all elements, Bi+V+Ti, (c) Ti, (d) Bi, and (e) V has been shown. A careful analysis reveals a uniform distribution of BVQDs, particularly on the pores on the edges and periphery of titania particles. In addition, somewhat lesser dense BVQDs are seen within the bigger particles of TiO_2. Distribution of BVQDs are particularly discernible in panel (b). This result is in good correlation with TEM and HRTEM results shown in Figure 3 in the main manuscript and Fig. S9.

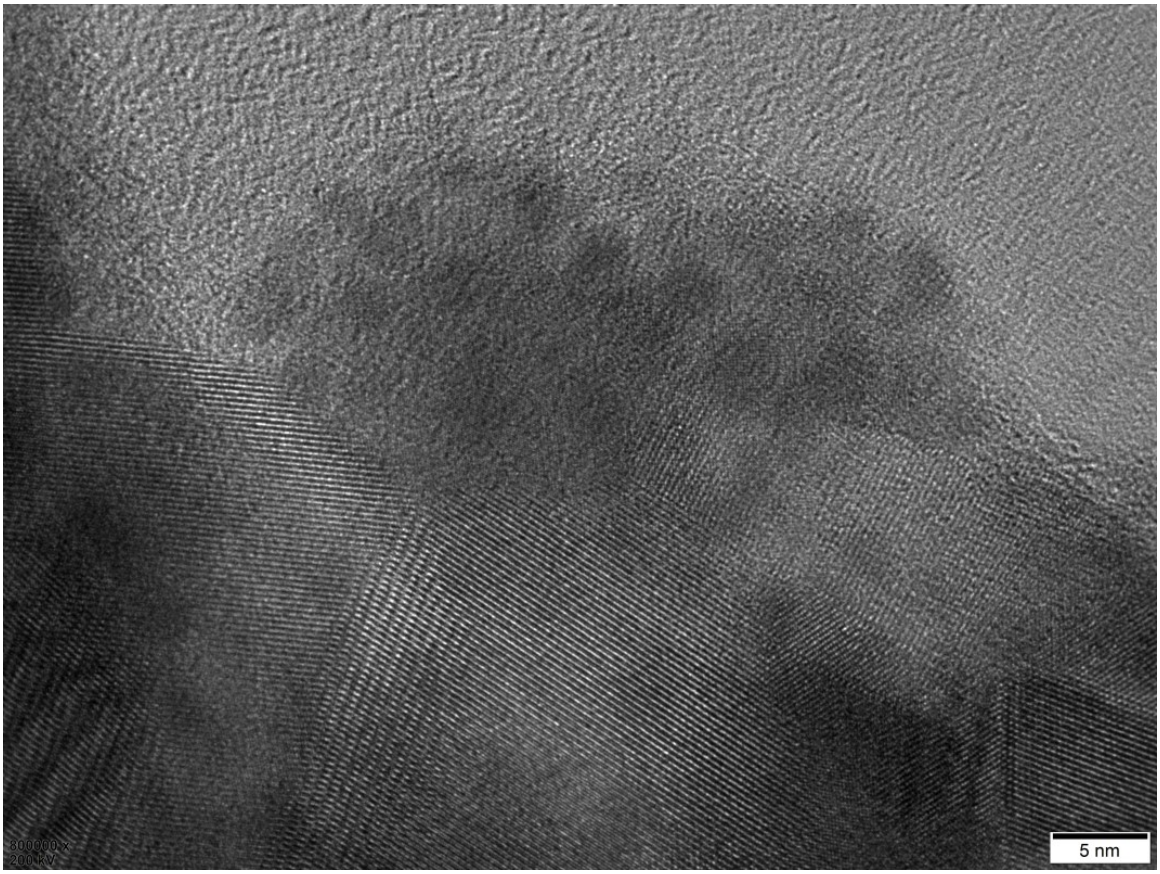

Figure S8: High resolution TEM image of BVT to show the filling of TiO_2 pores of 2.5±0.5 nm diameter with $BiVO_4$.

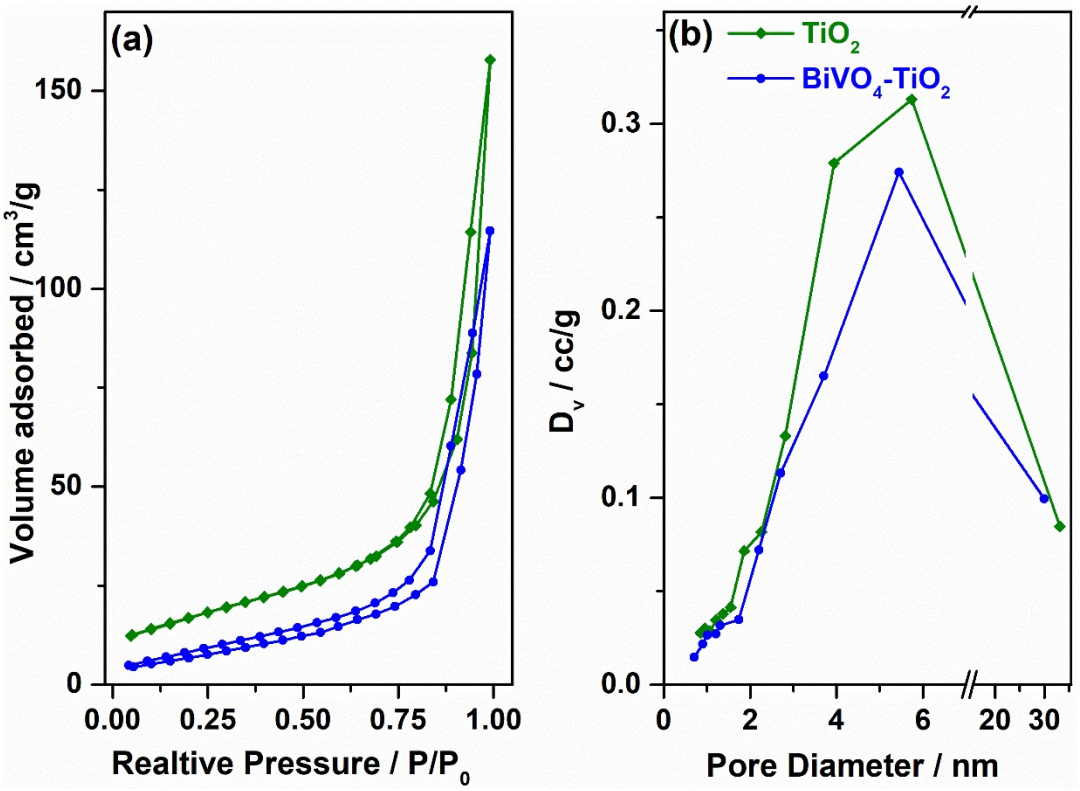

Figure S9: (a) N_2-adsorption-desorption isotherms, and (b) pore size distribution of TiO_2 and BVT. Contribution to pore volume comes in a major way from mesopores (> 2nm) and in a minor way from micropores (<2 nm) in both cases. Small, but significant decrease in pore volume of BVT, compared to TiO_2, is evident from the above results, which is attributed to the occupation of pores by BV QDs. Decrease in mesopores volume is directly evident. From the present results and the TEM observations, it is reasonable to assume a 20:80 ratio of weight percent of $BiVO_4$ distributed in smaller and bigger pores of 2.5 and 4 nm diameter in size. This is only to calculate the number of heterojunctions in a quick way and we assume a generous 10-20 % error.

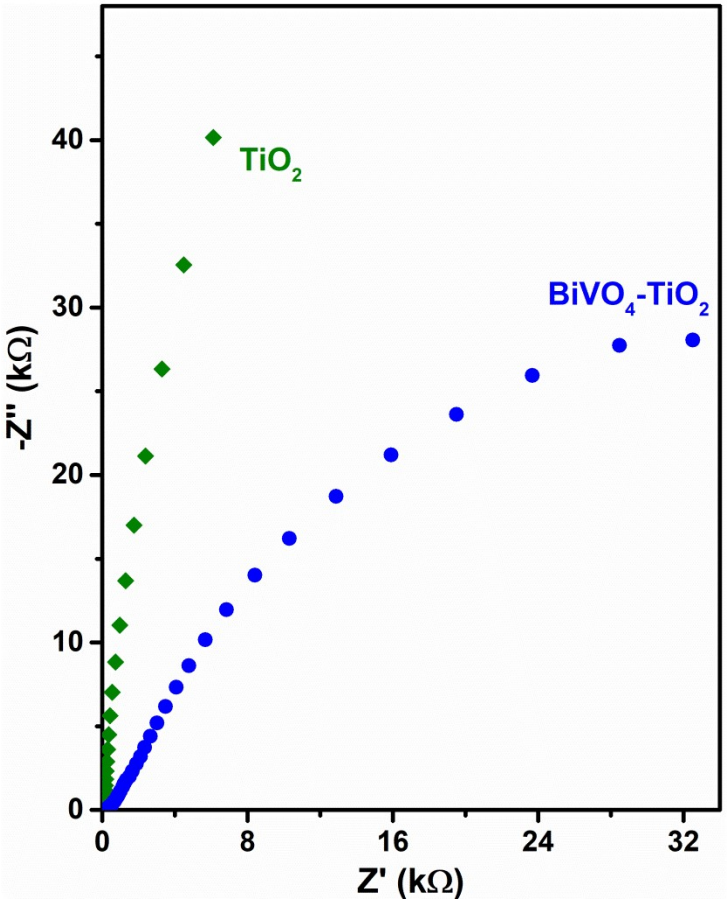

Figure S10: Electrochemical impedance spectroscopy (EIS) Nyquist plots, measured identically under one sun illumination with 0.5 M Na_2SO_4 solution, for TiO_2 and $BiVO_4$-TiO_2. Nyquist plot was measured from EIS to characterize charge carrier transfer properties between photoanode and electrolyte under one sun conditions. Smaller arc and impedance of Nyquist plot observed with BVT accounts for strong electron transport ability, while large impedance observed with TiO_2 shows high electron-hole pair recombination. Under light irradiation, smaller arc observed with BVT indicates that photogenerated charge carries are easily separated and transferred across interphase. While large electron-hole pair recombination with TiO_2 leads to high impedance.

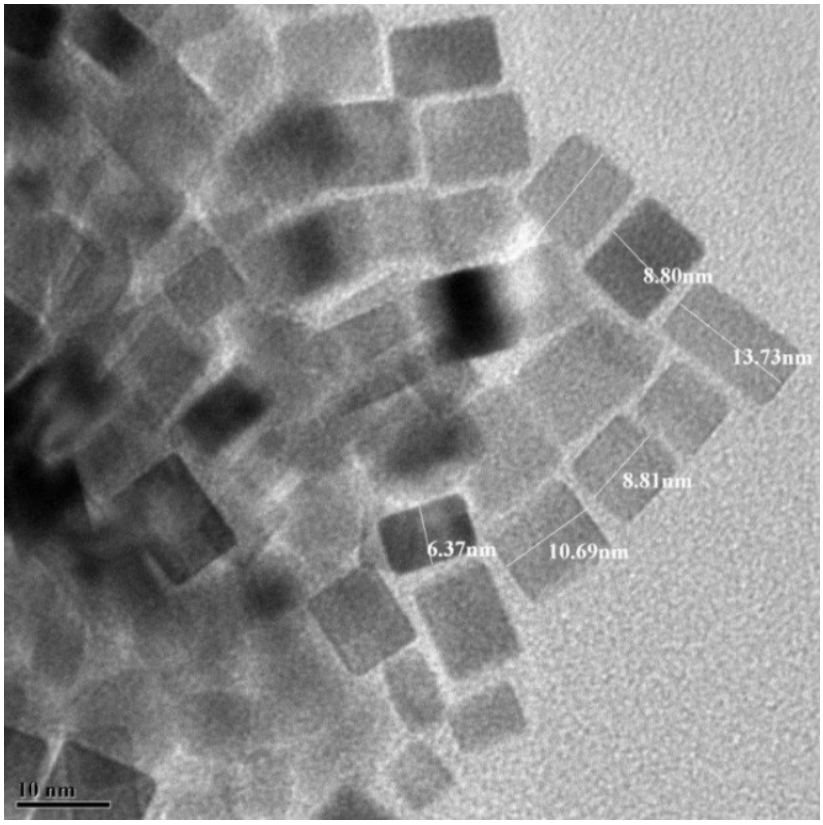

Figure S11: TEM image observed with Pd nanoparticles co-catalyst. 8-9 nm particle size was observed predominantly (80 %) and particle size range was observed between 6 and 13 nm.

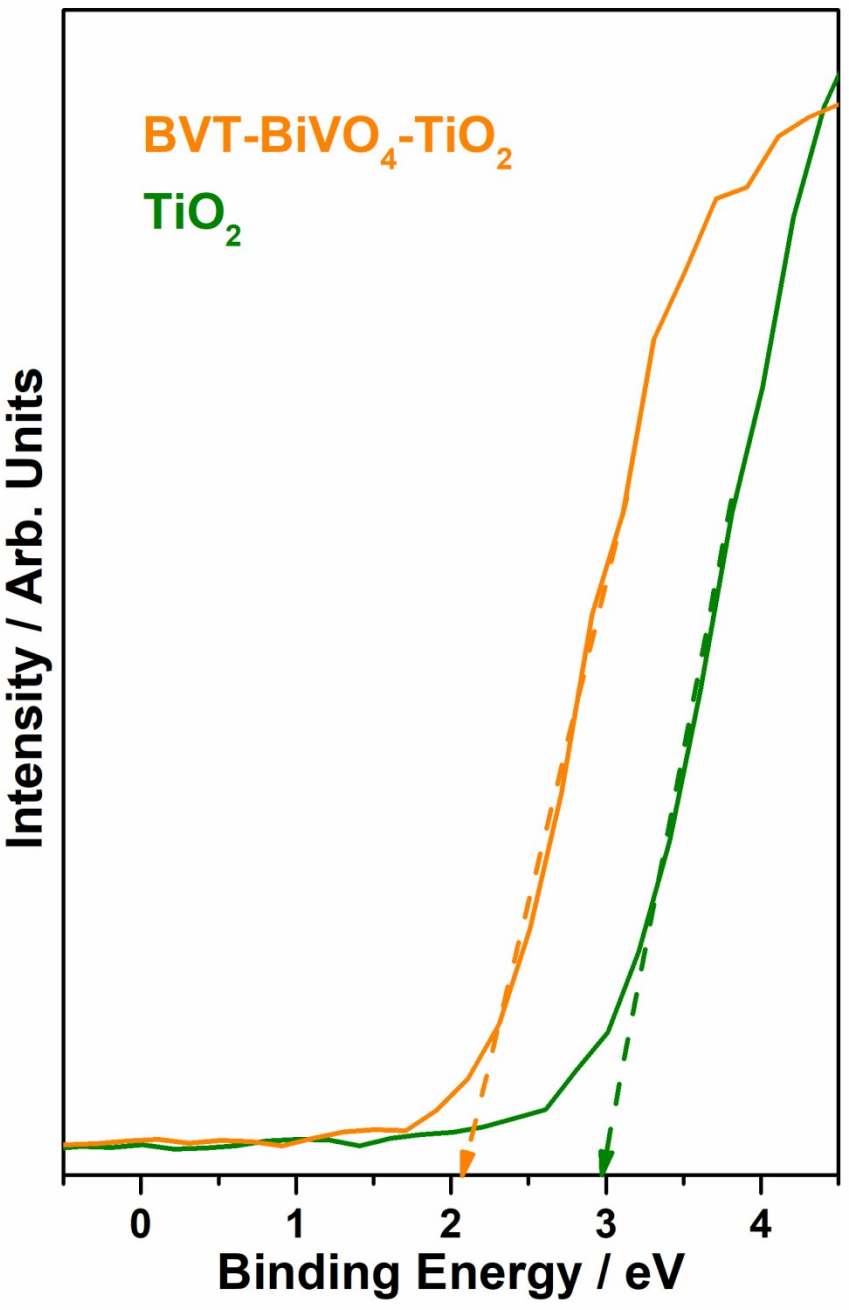

Figure S12: X-ray valence band spectra recorded for P25-TiO_2 and BVT, provides the VB_{Max} values. About 0.9 eV shift in VB edges underscores the electronic integration of $BiVO_4$ in the nanopores of TiO_2.

Table S1: We report the lattice parameters of bulk TiO_2, $BiVO_4$, and Pd calculated in this work and reported in experiments. Calculated lattice parameters agree well with the experimentally reported ones.

Bulk	Crystal structure	Lattice parameter calculated (Å)	Lattice parameter experimental (Å)[15,16,17]
TiO_2	Tetragonal	a= 3.79; c= 9.60	a= 3.78 and c= 9.50
$BiVO_4$	Monoclinic	a= 7.25; b= 11.59; c= 5.12	a= 7.25; b= 11.70; c= 5.09
Pd	FCC	a= 3.92	a= 3.89

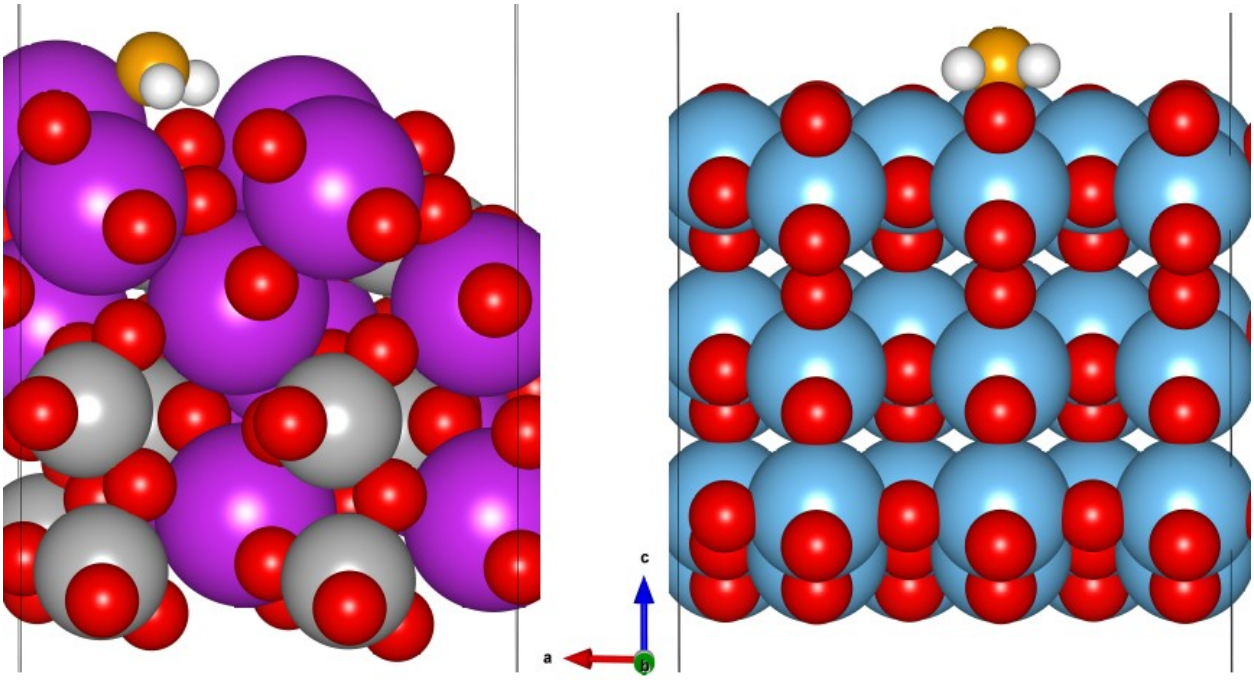

(a) H_2O on $BiVO_4(121)$ (b) H_2O on $TiO_2(101)$

Figure S13: Final adsorption geometries for H_2O over (a) $BiVO_4(121)$ and (b) $TiO_2(101)$ surface. H_2O strongly chemisorbs on $BiVO_4(121)$ with 8% bond activation and Bi-O bond distance 2.37 Å with E_{ads} = -1.43 eV whereas it moderately chemisorbs on TiO_2 (101) with 2% bond activation at a distance of 2.25 Å and with E_{ads} = -0.97 eV.

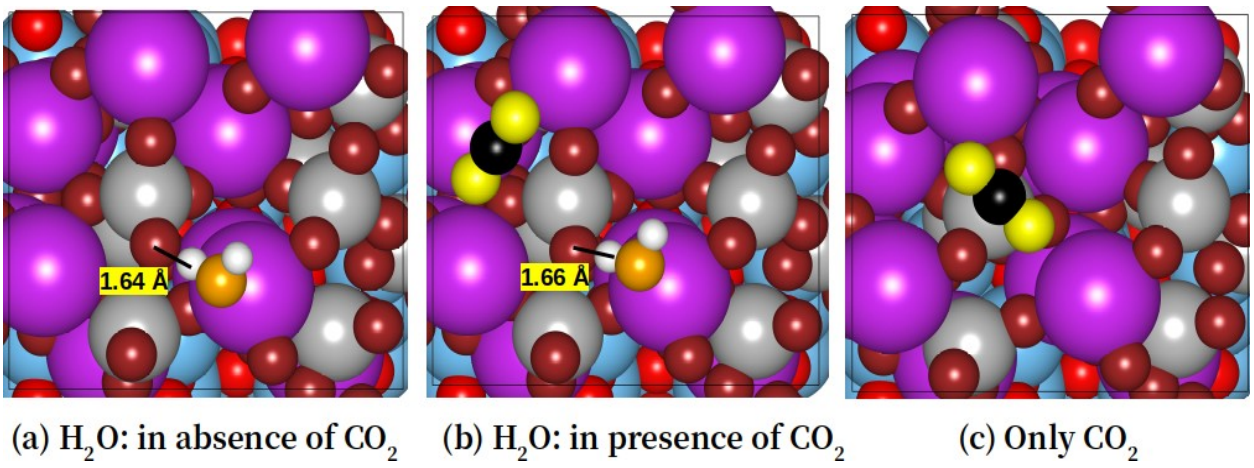

Figure S14: Thermodynamically most favorable geometries over $BiVO_4(121)/TiO_2(101)$ system. (a) adsorption of H_2O in absence of CO_2, (b) adsorption of H_2O in presence of CO_2, and (c) adsorption of CO_2. H_2O strongly interacts with the surface oxygen (O_s) with O_s-H = ~1.6 Å leading to surface reconstruction. With physisorption of CO_2 no surface reconstruction is observed. Color code used is H= white, O_H (O of H_2O) = golden yellow, C= black, and O_C (O of CO_2)= bright yellow.

Table S2: We report the shortest bond distance between the adsorbate and the surface for thermodynamically most favorable geometries. O-H1/H2 and C-O1/O2 refers to the bond length of H_2O and CO_2, respectively. E_{ads} is the adsorption energy. O_s refers to surface oxygen. H_2O is chemisorbed in presence or absence of CO_2 whereas CO_2 only physisorbs.

Adsorbate	Bi-H (Å)	O_s-H (Å)	H1-O (Å)	H2-O (Å)	HOH (°)	E_{ads} (eV)
H_2O	2.57	1.64	0.97	1.01	108	-1.96
H_2O+CO_2	2.60	1.66	0.98	1.01	106	-2.29
CO_2	V-C (Å)	O_s-C (Å)	C-O1 (Å)	C-O1 (Å)	OCO (°)	E_{ads} (eV)
	3.56	3.2	1.18	1.18	178	-0.47

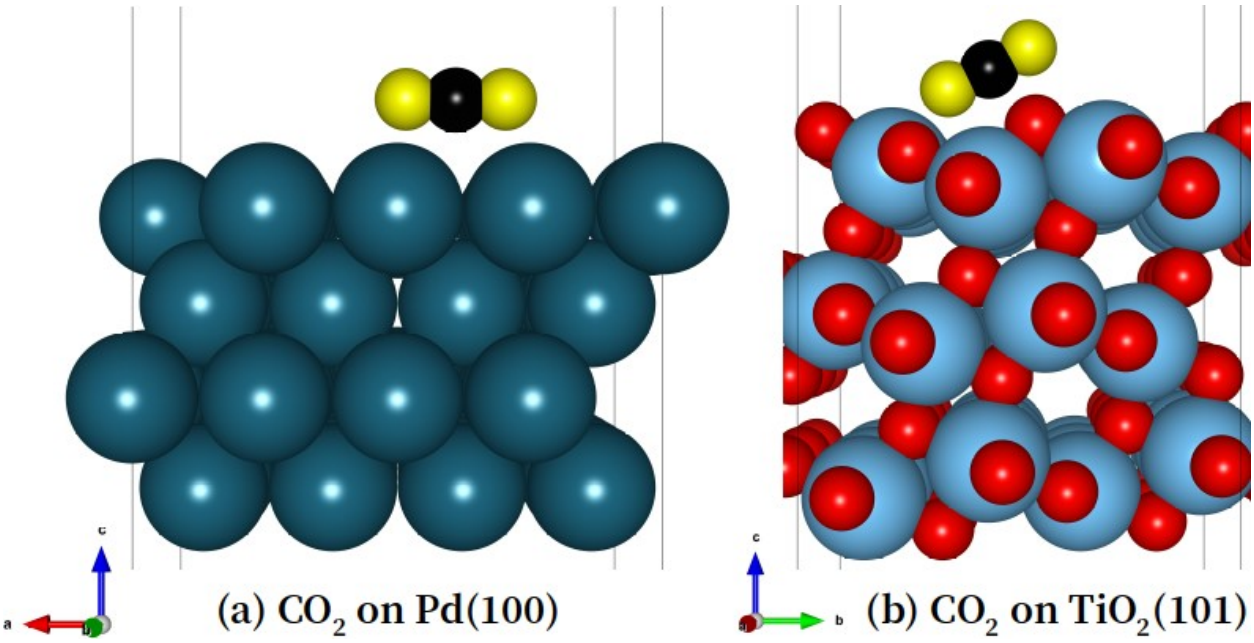

Figure S15: Adsorption geometries for CO_2 over pure (a) Pd(100) and (b) TiO_2(101) system. CO_2 is found to physiosorb in both the cases at a distance > 2.5 Å from the surface. In final geometry it is parallel to Pd(100) while tilted at TiO_2(101) with a slight bending of ∠ OCO by ~3° (177°).

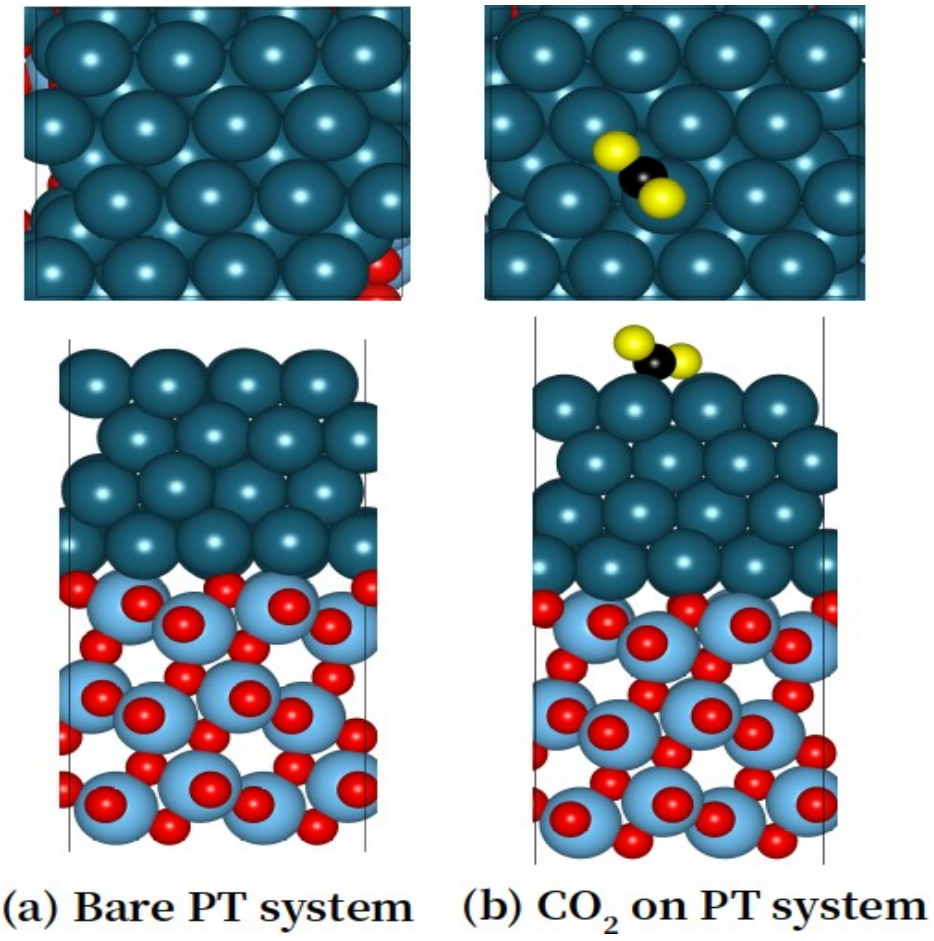

Fig. S16: Upper and lower panels are for top and side views. (a) Pd(100)/TiO_2(101) hetero-junction referred as PT. E_{form} of Pd(100)/TiO_2 (101) is calculated to be -9.11 eV. This also includes the energy associated with rearrangement of Pd atoms while formation of Schottky (metal-semiconductor Pd-TiO_2) junction, and (b) CO_2 chemisorbs in bent configuration over PT. The C-O bond elongation is 1.22 and 1.26 Å and ∠OCO is bent from its normal linear geometry by 42° (or to 138°).

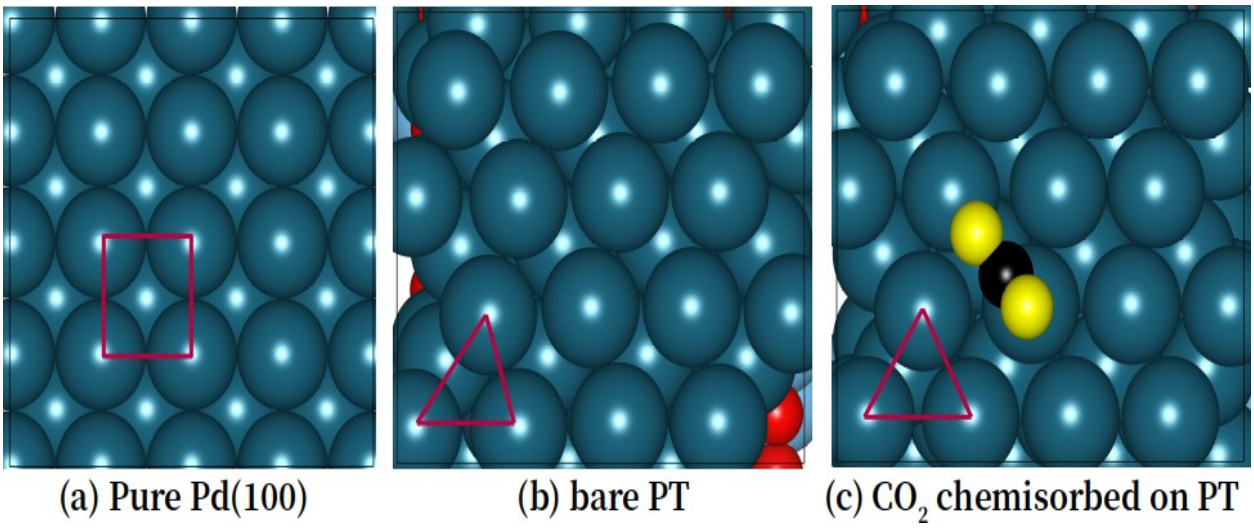

Figure S17: (a) Pure Pd(100), (b) bare Pd-TiO_2 (PT) Schottky junction, and (c) chemisorbed CO_2 over PT Schottky junction. Interfacing Pd(100) over TiO_2(101) leads to reconstruction at the surface. In presence of CO_2 the reconstruction is more evident and closely resembles to the (111) facet.

Table S3: Comparison of Mulliken charges (e-) for V ions at the interface versus in the pure $BiVO_4$(121). By convention a more positive value implies loss in charge. It is evident from the table that layer 2 and 3 that V ions loss more charge when hetero-junction is formed than when they are in pure $BiVO_4$(121) system. Refer to Fig. 8b.

Layer	BVT	$BiVO_4$(121)
1	1.38, 1.31, 1.25, 1.37	1.35, 1.35, 1.41, 1.41
2	1.15, 1.13, 1.27, 1.28	1.05, 1.05, 1.14,1.14
3	1.36, 1.25, 1.32, 1.43	1.19, 1.19, 1.35, 1.35

References:

1 M. Jin, H. Liu, H. Zhang, Z. Xie, J. Liu and Y. Xia, *Nano Res.*, 2011, **4**, 83–91.

2 N. Nalajala, K. K. Patra, P. A. Bharad and C. S. Gopinath, *RSC Adv.*, 2019, **9**, 6094–6100.

3 a) M. Qureshi and K. Takanabe, *Chem. Mater.*, 2017, **29**, 158–167. b) H. Kisch and D. Bahnemann, *J. Phys. Chem. Lett.*, 2015, **6**, 1907-1910.

4 I. Laraib, M. A. Carneiro and A. Janotti, *J. Phys. Chem. C*, 2019, **123**, 26752–26757.

5 J. K. Cooper, S. Gul, F. M. Toma, L. Chen, P. A. Glans, J. Guo, J. W. Ager, J. Yano and I. D. Sharp, *Chem. Mater.*, 2014, **26**, 5365–5373.

6 G. Kresse and J. Hafner, *Phys. Rev. B*, 1994, **49**, 14251–14269.

7 G. Kresse and J. Furthmüller, *Phys. Rev. B - Condens. Matter Mater. Phys.*, 1996, **54**, 11169–11186.

8 G. Kresse and J. Furthmüller, *Comput. Mater. Sci.*, 1996, **6**, 15–50.

9 S. Grimme, *J. Comput. Chem.*, 2006, **27**, 1787–1799.

10 A. Jain, S. P. Ong, G. Hautier, W. Chen, W. D. Richards, S. Dacek, S. Cholia, D. Gunter, D. Skinner, G. Ceder and K. A. Persson, *APL Mater.*, , DOI:10.1063/1.4812323.

11 D. Stradi, L. Jelver, S. Smidstrup and K. Stokbro, *J. Phys. Condens. Matter*, , DOI:10.1088/1361-648X/AA66F3.

12 J. Heyd, G. E. Scuseria and M. Ernzerhof, *J. Chem. Phys.*, 2006, **124**, 219906.

13 J. Heyd, G. E. Scuseria and M. Ernzerhof, *J. Chem. Phys.*, 2003, **118**, 8207.

14 S. Maintz, V. L. Deringer, A. L. Tchougréeff and R. Dronskowski, *J. Comput. Chem.*, 2016, **37**, 1030–1035.

15 J. K. Burdett, T. Hughbanks, G. J. Miller, J. V. Smith and J. W. Richardson, *J. Am. Chem. Soc.*, 1987, **109**, 3639–3646.

16 A. W. Sleight, H. y. Chen, A. Ferretti and D. E. Cox, *Mater. Res. Bull.*, 1979, **14**, 1571–1581.

17 S. Pati, R. A. Jat, S. K. Mukerjee and S. C. Parida, *Physica. B. Condens. Matter*, 2016, **484**, 42–47.